nature communications

Article

https://doi.org/10.1038/s41467-025-61166-6

Impedance decoupling strategy to enhance the real-time powering performance of TENG for multi-mode sensing

Received: 9 January 2025

Accepted: 12 June 2025

Published online: 01 July 2025

Check for updates

Hao Sun[1,3], Yuxuan Xia[1,3], Jinyan Zhi[1,3], Jun Ma[1], Jinwan Chen[1], Zhekai Chu[1], Weihao Gao[2], Shuhai Liu[1,2] ✉ & Yong Qin[2] ✉

Triboelectric nanogenerator can scavenge mechanical energy from environment to power sensor networks, becoming increasingly important in fields like healthcare and infrastructure. However, due to its impedance coupling with sensor networks, stimuli-induced impedance changes of sensor networks will result in an inconstant output of triboelectric nanogenerator, leading to a poor real-time powering performance for sensor networks as compared with a constant voltage source; designing triboelectric nanogenerator with high powering performance to real-timely power sensor networks faces great challenges. Herein, an impedance decoupling strategy is proposed to enhance the real-time powering performance of triboelectric nanogenerator by decoupling impedances of triboelectric nanogenerator and sensor network. A shunt circuit composed of a small fixed resistor is introduced to stabilize the whole impedance of the shunt circuit and the sensor network, making the output voltage of triboelectric nanogenerator on sensors almost unchanged, and thus cut off the impedance coupling. Our results show that the strategy highly enhances the real-time powering performance of triboelectric nanogenerator for sensor networks, and achieves multi-mode sensing with relative errors as low as −4.6%, comparable to that powered by a commercial power source. This work provides useful guidance for designing triboelectric nanogenerator for multi-mode sensing, and contributes to its practical applications.

The rapid development of the Internet of Things and artificial intelligence[1,2] has immense impacts on various aspects of wearable sensing[3,4], skin electronics[5,6], environmental monitoring[7], in which sensing technology plays an important role. Seeking of a suitable power source for sensor networks composed of widely distributed sensors is becoming increasingly important. The current powering technology for widely distributed sensors still relies on batteries. Because batteries need to be replaced, recharged and recycled regularly, increasing maintenance costs, and a large number of battery nodes are prone to environmental pollution, powering widely distributed sensors with batteries is a challenge or even impossible[8]. In order to meet this challenge, self-powered sensing technology[9–12] was proposed that utilizes triboelectric nanogenerator (TENG) to scavenge high-entropy energy widely distributed in the environment to power the widely distributed sensors (Fig. 1a) without the need for external batteries, which has received worldwide attention in the past years.

For real-timely powering sensor networks, the traditional strategy (TS) is to connect TENG directly with sensors (Fig. 1b). The biggest advantage of TS is that the self-powered system composed of TENG and sensor networks has a simple structure and strong universality

[1]Institute of Nanoscience and Nanotechnology, School of Materials and Energy, Lanzhou University, Lanzhou, Gansu, China. [2]MIIT Key Laboratory of Complex-field Intelligent Exploration, Beijing Institute of Technology, Beijing, China. [3]These authors contributed equally: Hao Sun, Yuxuan Xia, Jinyan Zhi.
✉e-mail: liushuhai1991@live.cn; qinyong@lzu.edu.cn

https://doi.org/10.1038/s41467-025-61166-6

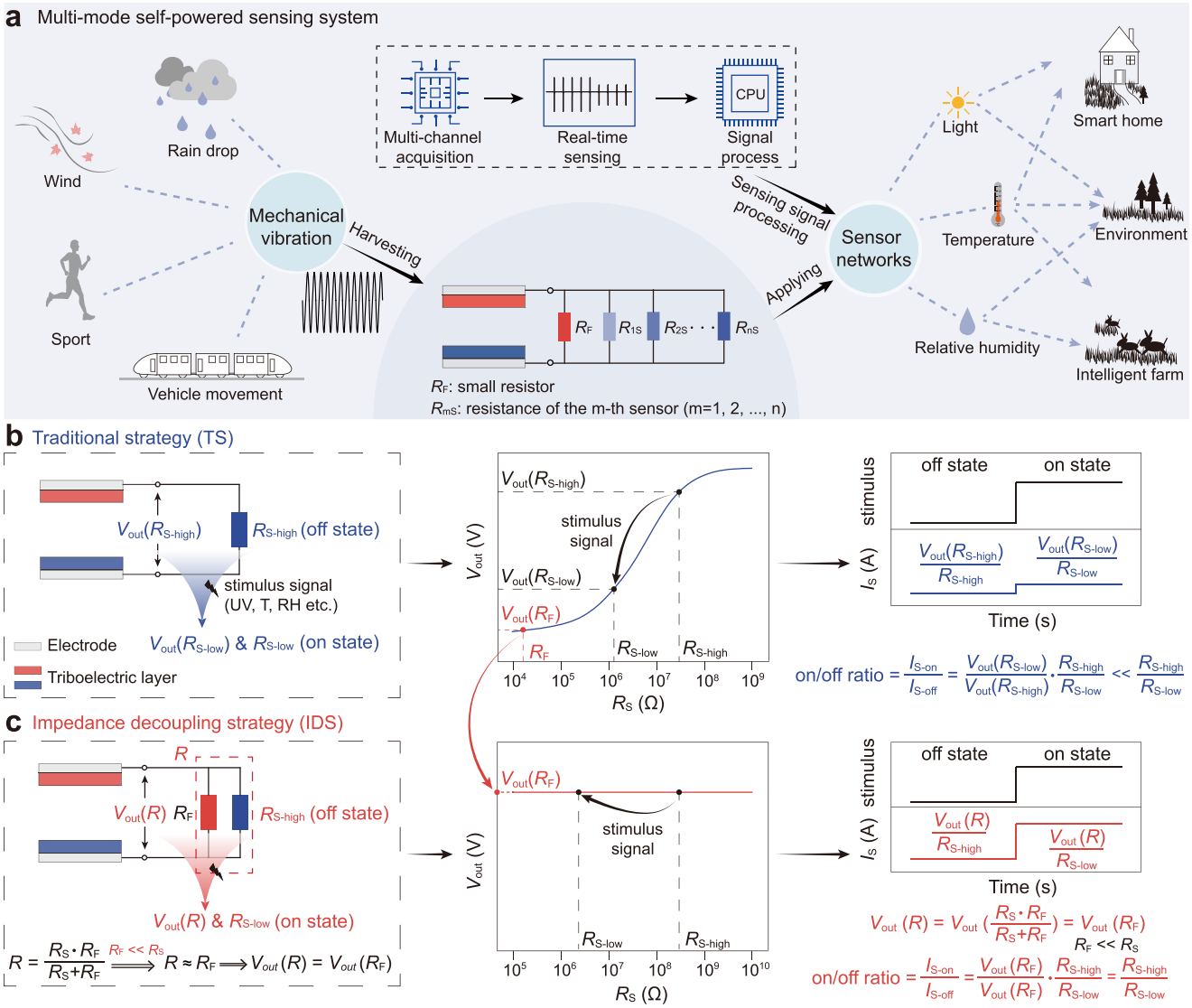

Fig. 1 | Working mechanism of impedance decoupling strategy (IDS). **a** Conceptual framework for the application of sensor network based on the multi-mode self-powered sensing system. **b**, **c** Mechanism diagrams of traditional strategy (TS, **b**) and IDS (**c**). Due to triboelectric nanogenerator's impedance-dependent output voltage characteristics, the on/off ratio of sensor measured by TS is much smaller than the on/off ratio of the actual. The purpose of the IDS is to stabilize the voltage at both ends of the sensor: the output voltage $V_{out}(R)$ is unchanged before and after the sensor is stimulated, and the value is equal to $V_{out}(R_F)$, so the on/off ratio of sensor measured by IDS is almost equal to the on/off ratio of the actual.

suitable for various sensing scenarios, and can provide real-time power source for sensors[13–15]. However, TS will degrade the real-time powering performance of TENG compared to a constant voltage source (CVS), resulting in poor real-time sensing performance (i.e., on/off ratio) of the self-powered system. The main reason of this degraded real-time powering performance of TENG mainly comes from the load impedance-dependent output characteristics of TENG, which more fundamentally results from the impedance coupling between the TENG and the sensor networks (as loads). Under a stimulus (e.g., light, temperature, and force) to be detected, the sensor resistance will decrease (or increase), and simultaneously results in a decrease (or increase) of the TENG output voltage; as a result, these two variations together lead to the sensing on/off ratio of self-powered system being much smaller than its intrinsic sensing on/off ratio, i.e., poor powering performance of TENG and poor sensing performance of self-powered system. This challenge remains unsolved for a long time; until recently, a second-best solution of synchronous switching strategy was proposed by us[16], in which a synchronous switch was introduced to physically disconnect TENG and sensor during the process of charge accumulation, and connect them during instantaneous discharge, thus to decouple their impedances. Although this synchronous switching strategy provides a guidance to achieve a load-independent output voltage to highly enhance the real-time powering performance of TENG, it currently only suitable for instantaneous discharging TENG, and more importantly, relies on signal acquisition with an ultra-high sampling rate as high as 10^5 sps (unit: sample per second), and in fact has poor universality and poor scenario adaptability. Up to now, finding universal strategies to make TENG has higher powering performance to real-timely power sensor networks is one of the most pressing challenges in the field.

In this work, a simple but universal impedance decoupling strategy (IDS) is proposed to enhance the real-time powering performance of TENG. IDS only needs to introduce a shunt circuit composed of a small fixed resistor to stabilize the whole load impedance and thus to cut off the impedance coupling between TENG and sensor network. This strategy is almost as simple as TS, but simultaneously, it has no relation with the instantaneous discharging TENG, in other words, it is a universal high performance powering strategy for all types of TENG.

Our theoretical, computational and experimental results show that IDS enables TENG to real-timely power various commercial sensors, such as temperature sensors and opto-sensors, and achieve relative errors as low as −4.6%. Moreover, a self-powered system based on IDS is successfully constructed for multi-mode sensing that can simultaneously monitor temperature and light intensity without any crosstalk from each other, and achieves sensing performance (i.e., on/off ratio) comparable to that powered by a commercial CVS. This work greatly increases the real-time powering performance of TENG, which is expected to promote the practical application of TENG.

Results

Working mechanism of IDS

Figure 1a illustrates the important application scenarios of self-powered system composed of TENG and sensor networks in smart home, environmental monitoring and intelligent farm, et al. TENG harvests mechanical energy from environment for powering sensor networks and captures multi sensing signals. Due to the impedance coupling between TENG and sensor (as load), the output ($V_{out}(R)$, $I_{out}(R)$) of TENG strongly depends on the sensor impedance (R)[17–19].

In TS, the TENG is directly connected to the sensor (R_S) as shown in Fig. 1b. Taking the case that R_S decreases under stimuli as an example, when the sensor is unstimulated (off state, $R_{S\text{-high}}$) and stimulated (on state, $R_{S\text{-low}}$), the output voltage of TENG is $V_{out}(R_{S\text{-high}})$ and $V_{out}(R_{S\text{-low}})$, respectively. Then, the on/off ratio obtained by TS can be expressed as:

$$\begin{aligned}\text{on/off ratio} &= \frac{I_{S-on}}{I_{S-off}} = \frac{V_{out}(R_{S-low})/R_{S-low}}{V_{out}(R_{S-high})/R_{S-high}} \\ &= \frac{V_{out}(R_{S-low})}{V_{out}(R_{S-high})} \bullet \frac{R_{S-high}}{R_{S-low}} \neq \frac{R_{S-high}}{R_{S-low}}\end{aligned} \tag{1}$$

where $I_{S\text{-on}}$ and $I_{S\text{-off}}$ represents the current flowing through the sensor when the sensor is on state and off state, respectively. Because $V_{out}(R_{S\text{-low}})$ is not equal to $V_{out}(R_{S\text{-high}})$, the obtained on/off ratio by TS is not equal to the intrinsic one ($R_{S\text{-high}}/R_{S\text{-low}}$), resulting in inaccurate sensing. As can be seen, it is the impedance coupling between TENG and sensor that fundamentally leads to the poor sensing performance, which means that the powering performance of TENG in TS is poor.

To solve above problem, as shown in Fig. 1c, when a shunt circuit composed of a small fixed resistor (R_F) is introduced in IDS to cut-off the impedance coupling between TENG and sensor, the whole load impedance $R = R_S \bullet R_F/(R_S + R_F)$, calculated by the parallel resistance of R_S and R_F, is approximately equal to R_F when $R_F \ll R_S$. In this case, the output voltage of TENG can be expressed as:

$$V_{out}(R) = V_{out}\left(\frac{R_S \bullet R_F}{R_S + R_F}\right) \approx V_{out}(R_F). \tag{2}$$

The on/off ratio obtained by IDS can be expressed as:

$$\begin{aligned}\text{on/off ratio} &= \frac{I_{S-on}}{I_{S-off}} = \frac{V_{out}\left(\frac{R_{S-low} \bullet R_F}{R_{S-low} + R_F}\right)/R_{S-low}}{V_{out}\left(\frac{R_{S-high} \bullet R_F}{R_{S-high} + R_F}\right)/R_{S-high}} \\ &\approx \frac{V_{out}(R_F)}{V_{out}(R_F)} \bullet \frac{R_{S-high}}{R_{S-low}} = \frac{R_{S-high}}{R_{S-low}}\end{aligned} \tag{3}$$

This formula shows that the impedance coupling between the TENG (internal impedance Z_i) and the sensor (R_S) is cut off by R_F, so the on/off ratio obtained by IDS is equal to intrinsic on/off ratio. In theory, accurate sensing stimuli can be measured by IDS rather than TS.

It should be noted that the above derivation and analysis are based on, but not limited to sensors whose resistance decreases with stimulus, they are also suitable for sensors whose resistance increases with stimulus. Moreover, the above theoretical results are also applicable to the case of simultaneously powering multi-mode sensing by TENG in IDS (Supplementary Note 1 and Supplementary Fig. 1). It is worth noting that in IDS, there is no crosstalk between multiple sensors, conducive to promoting high-level applications of TENG in self-powered system for multi-mode sensing.

Dynamic simulations of TENG in TS and IDS

To verify the validity of IDS, a dynamic finite element simulation model was constructed by a 'moving mesh' method[16] to simulate the self-powered sensing performed in TS (for comparison) and IDS. The powering performances of TENG in TS and IDS with various sensor resistances (R_S) are respectively simulated in Fig. 2a, b. In TS, $V_{out}(R_S)$ increases with increase of R_S and becomes stable at about $10^6\ \Omega$, which means that the accurate on/off ratio can be obtained by TS when R_S is greater than $10^6\ \Omega$. It is worth noting that this is limited to the Z_i of TENG is about $5 \times 10^3\ \Omega$, while the Z_i of TENG in actual experiments ranges from about 10^6 to $10^8\ \Omega$[20–22], which is much higher than the Z_i of TENG in simulation, so it is difficult to have a sensor matching TENG and obtain their accurate on/off ratio by TS. For comparison, in IDS, $V_{out}(R_S)$ remains stable after R_S is greater than $10^2\ \Omega$ when R_F is $10\ \Omega$. This indicates that when R_S is greater than $10^2\ \Omega$, the accurate on/off ratio can be obtained by IDS, and indicating that IDS is suitable for a large R_S range. The relationship between R_F and TENG output ($V_{out}(R)$, $I_{out}(R)$) is shown in Supplementary Fig. 2 (Supplementary Note 2).

In addition, the sensing performance of self-powered system respectively based on TS and IDS are also simulated. Here, we take an opto-sensor as an example, set R_F of $10\ \Omega$ and assume that R_S are $5 \times 10^4\ \Omega$, $5 \times 10^3\ \Omega$ and $5 \times 10^2\ \Omega$ under dark, weak and strong illumination, respectively. As shown in Fig. 2c, the on/off ratio obtained by TS after weak and strong illumination is respectively about 6.6 (weak illumination) and 17.0 (strong illumination), which are much lower than the actual ones (10 for weak illumination, 100 for strong illumination); while, the on/off ratio obtained by IDS is about 10.0 (weak illumination, ~ 10) and 98.1 (strong illumination, ~ 100) under same light conditions. This indicates that the sensing performance of self-powered system based on IDS is better than TS. To further find out the application scope of IDS, the on/off ratios obtained by TS and IDS as functions of the off-state R_S with intrinsic on/off ratio of 10, 10^2, 10^3, 10^4, 10^5 are shown in Fig. 2d and Supplementary Fig. 3 (Supplementary Note 3). Compared with TS, IDS is suitable for sensors with a wider resistance range. This further indicates that the powering performance of TENG is enhanced by IDS.

Moreover, the relationship between R_F and on/off ratio is also simulated in Fig. 2e and Supplementary Fig. 4 (Supplementary Note 4). When R_F is much smaller than R_S, the on/off ratio obtained by IDS is much closer to the intrinsic on/off ratio; while, with the increase of R_F, formula (3) is not valid due to $V_{out}(R) \neq V_{out}(R_F)$, and the on/off ratio obtained by IDS is inaccurate. As a result, the on/off ratio decreases with the increase of R_F, and the off-state R_S becomes larger, and R_F becomes smaller. This also shows that, from another perspective, R_F should be properly selected according to the sensor characteristics (i.e., off-state R_S, and intrinsic on/off ratio), and the on/off ratio reaches higher than 90% of the intrinsic on/off ratio when $R_{S\text{-min}} \geq 10R_F$ (Supplementary Fig. 5, Supplementary Note 5 and Supplementary Table 1). The stability measurement of IDS is also simulated in Fig. 2f. The on/off ratio obtained by TS increases with the increase of approaching frequency (f) of two triboelectric layers, and the on/off ratio obtained by IDS is always around 9.9, which is the same as the intrinsic on/off ratio 10.0. So, IDS can enhance the powering performance of TENG not only working at low frequency but also at high frequency. (Supplementary Fig. 6 and Supplementary Note 6). In addition, the on/off ratio by IDS as functions of surface charge density and dielectric constant of triboelectric layers are both investigated in Supplementary Fig. 7 (Supplementary Note 7). In brief, the on/off ratio obtained by IDS is not

https://doi.org/10.1038/s41467-025-61166-6

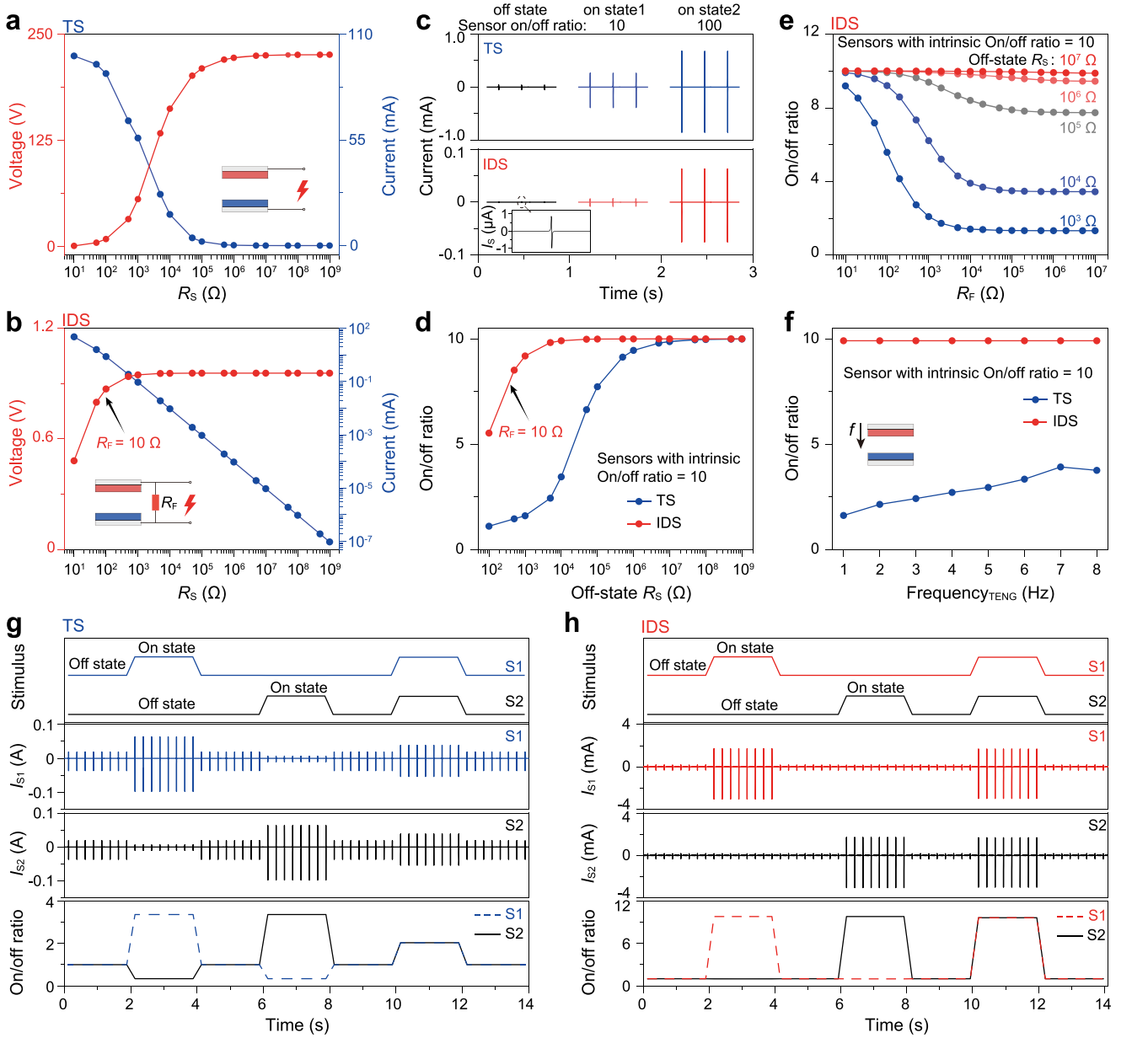

Fig. 2 | Dynamic simulations of triboelectric nanogenerator (TENG) in traditional strategy (TS) and impedance decoupling strategy (IDS). a, **b** Output voltage and output current of TENG in TS (**a**) and IDS (**b**) with different sensor resistance R_S. **c**, **d** Simulated off and on real-time sensing signals (**c**) and on/off ratios (**d**) of sensors powered by TENG in TS and IDS. IDS is suitable for a wider R_S range than TS. Inset: enlarged detail of the output current. **e** On/off ratios obtained by TS and IDS under different fixed resistor (R_F). Compared with R_S, the smaller the R_F, the better to achieve high-precision sensing. **f** On/off ratios obtained by TS and IDS under different contact frequencies of TENG triboelectric layers. **g**, **h** Simulated dynamic current (I_{S1} and I_{S2}) of multi-mode sensing in TS (**g**) and IDS (**h**). Two sensors influence each other in TS, and works independently in IDS. The sensors in simulations have an intrinsic on/off ratio of 10.

affected by approaching frequency, surface charge density, and materials of triboelectric layer, indicating that IDS is a universal strategy for TENG that does not influence by special driving modes or materials.

More importantly, the multi-mode sensing performance of self-powered system based on TS and IDS is further investigated in Figs. 2g, h, respectively. Sensor network for multi-mode sensing made of opto-sensor (R_{S1}) and temperature-sensor (R_{S2}) is taken as example, and the stimulus applied is shown in the upper of Fig. 2g. In TS, when only light is applied, the current of opto-sensor (I_{S1}) increases by 3.4 times, and the current of temperature sensor (I_{S2}) decreases. I_{S1} and I_{S2} increase with thermal and light stimuli are applied simultaneously, and the on/off ratio of two sensors is 2.0, which is less than the actual value 10.0. It shows that multiple sensors in TS will influence each other, resulting in inaccurate sensing for the stimulus. On the contrary, in IDS, I_{S1} increases by 9.8 times, and I_{S2} is unchanged, with only light is applied. When thermal and light stimuli are applied simultaneously, both I_{S1} and I_{S2} have increased 9.7 times, approximately equal to the intrinsic on/off ratio 10.0. A detail should be noted: two sensing signals have no crosstalk with each other; in other words, they are decoupled. These results further indicate that IDS can cut off the impedance coupling between TENG and sensor network by R_F, enhancing the real-time powering performance of TENG for multi-mode sensing, which is not possible in the past.

Enhanced powering performance of TENG by IDS

The powering performance of TENG in IDS is also investigated by comparing the output characteristics of TS and IDS in Fig. 3. In TS, the

https://doi.org/10.1038/s41467-025-61166-6

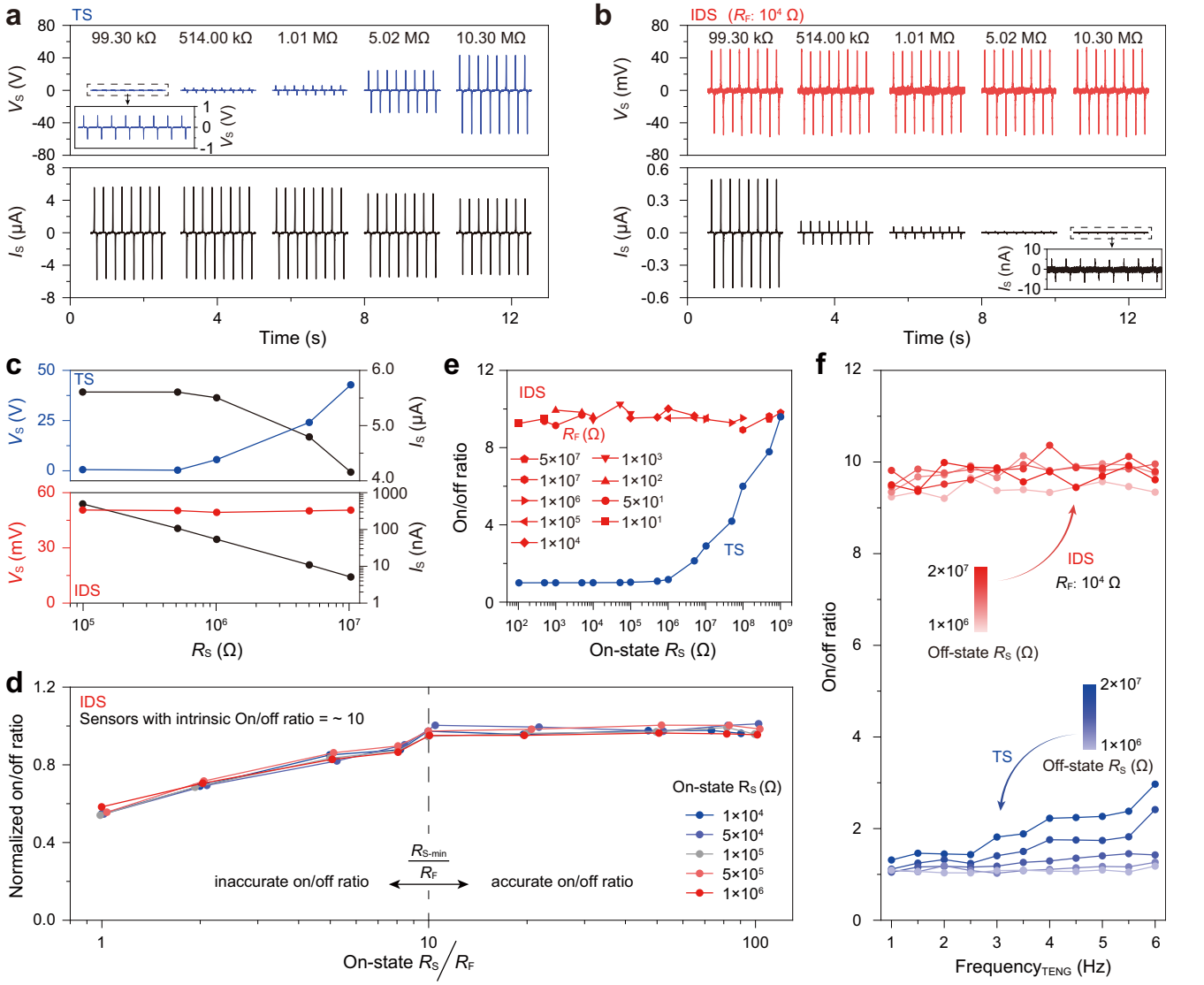

Fig. 3 | Enhanced powering performance of triboelectric nanogenerator (TENG) by impedance decoupling strategy (IDS). a, **b** Dynamic output voltage and output current of TENG in traditional strategy (TS, **a**) and IDS (**b**) with different sensor resistance (R_S). **c** output voltage and output current of TENG in TS and IDS varies with R_S summarized from a and b. Voltage measured by IDS stable with increasing R_S and current decreases. **d** Normalized on/off ratios measured by IDS under different fixed resistors (R_F). When the ratio of $R_{S\text{-min}}$ to R_F exceeds 10, the on/off ratio of sensor measured by IDS is accurate. **e**, On/off ratio of sensors measured by TS and IDS varies with on-state R_S (10^2–10^9 Ω). On/off ratio of sensors measured by IDS is accurate when R_F is selected properly. **f**, On/off ratios obtained by TS and IDS under different contact frequencies (f) of TENG triboelectric layers. On/off ratios measured by IDS is insensitive to f, and while on/off ratio measured by TS varies with f and is smaller than that measured by IDS.

dynamic voltage (V_S) and current (I_S) across the sensor, also equal to the TENG output, as a function of R_S are shown in Fig. 3a. It can be observed that, with the increase of R_S, I_S first remains stable and then decreases, and V_S keeps increasing. As a contrast, in IDS, when R_F are 10^4, V_S and I_S as functions of R_S are shown in Fig. 3b. A universal characteristic is that with the increase of R_S, I_S continuously decreases, while V_S increases first and then remains stable. It is worth noting that the voltage across R_S is stabilized to ~50 mV. The V_S and I_S across the sensor measured by TS (Fig. 3a) and IDS (Fig. 3b) are summarized in Fig. 3c. In IDS, when R_F is 10^4 Ω, the voltage remains stable when R_S is between 10^5 Ω and 10^7 Ω, and the current flowing through the sensor varies almost linearly with increasing R_S. In other words, the accuracy on/off ratios of R_S obtained by IDS when R_S is between 10^5 and 10^7 Ω. Additionally, R_F are 2.5×10^3, 5×10^3, and 2×10^4, V_S and I_S as functions of R_S are shown in Supplementary Fig. 8 (Supplementary Note 8). A universal characteristic is that with the increase of R_S, I_S continuously decreases, while V_S increases first and then remains stable. Moreover, the relationship between R_F and R_S is further investigated when IDS can obtain accurate on/off ratio of sensor (Fig. 3d). These results prove that on/off ratio measured by IDS can exceeds 90% of the intrinsic on/off ratio when $R_{S\text{-min}}/R_F \geq 10$, which is consistent with the simulations in Supplementary Fig. 5. With the increase of $R_{S\text{-min}}/R_F$, an abnormal phenomenon appears, that is, the on/off ratio measured by IDS is not accurate. A reasonable explanation is that, with the increase of R_S, the current gradually drops to 10^{-10} A, and I_S measurement is not easy to be accurate, resulting in inaccurate sensing (Supplementary Fig. 8 and Supplementary Note 8). In short, R_F is not the smaller the better, its optimal value is one-tenth of $R_{S\text{-min}}$. These observations indicate that IDS can effectively enhance the powering performance of TENG. Since most kinds of sensors have R_S in the range of 10^4–10^8 Ω[23–26], the powering performance of TS and IDS were studied over a larger sensor resistance range (10^2–10^{10} Ω) in Fig. 3e. The on/off ratio measured by TS keeps constant (~1) with the increase of R_S, increases gradually when R_S exceeds 10^6 Ω, and almost

https://doi.org/10.1038/s41467-025-61166-6

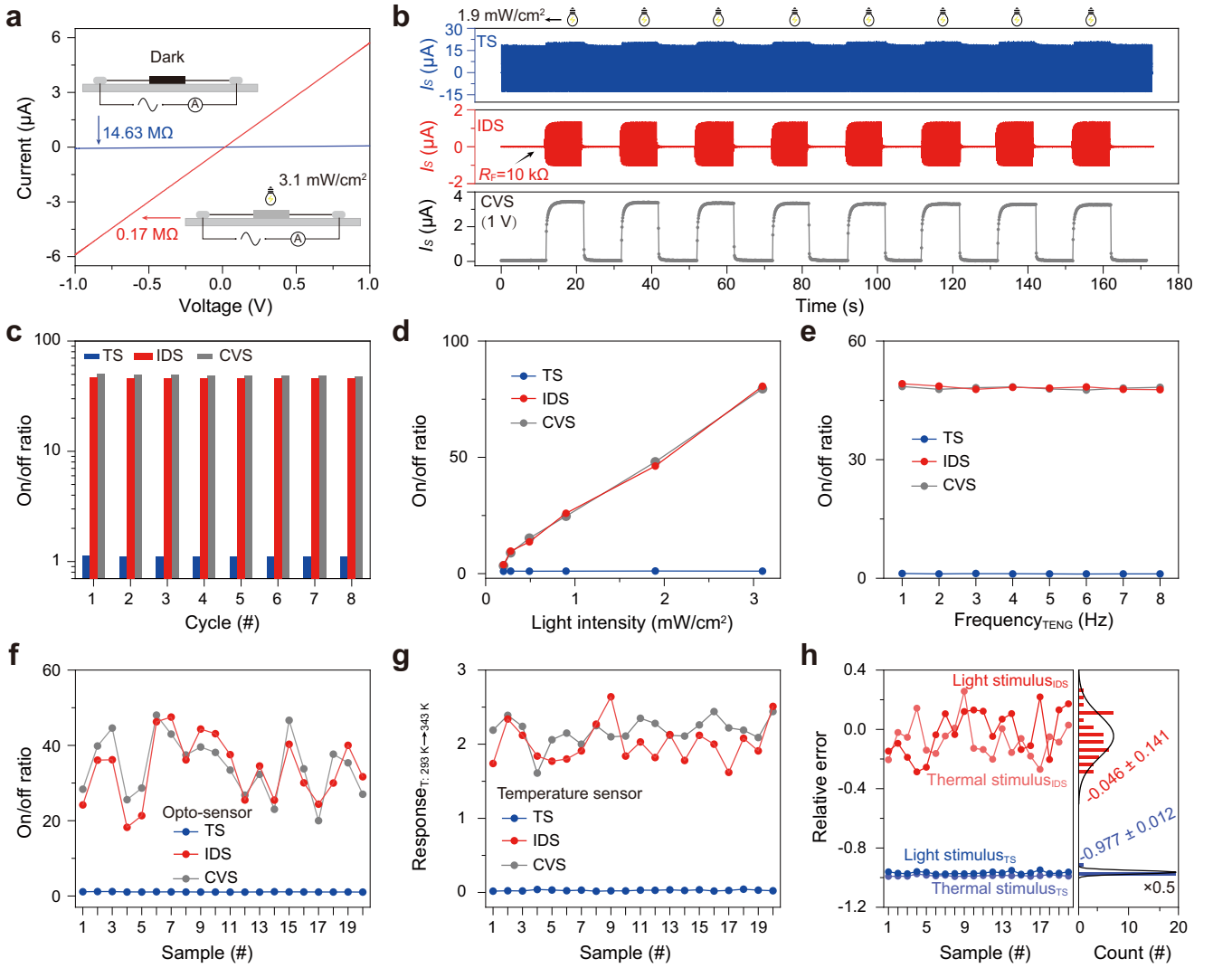

Fig. 4 | Practical demonstration of impedance decoupling strategy (IDS). a *I-V* characteristics of a commercial opto-sensor powered by a constant voltage source (CVS). **b** Dynamic current I_S of the opto-sensor measured by traditional strategy (TS), IDS and CVS with light intensity switched between dark and 1.9 mW/cm^2. **c** Summarized on/off ratios of opto-sensor measured by TS, IDS and CVS from (**b**). **d**, **e** On/off ratios of commercial opto-sensor powered by TS, IDS and CVS under different light intensities and different contact frequencies of TENG triboelectric layers, respectively. **f**, **g** Comparison of on/off ratios measured by TS, IDS and CVS using 20 commercial opto-sensors (**f**) and 20 commercial temperature sensors (**g**), respectively. **h** Summarized relative errors from (**f**, **g**).

equal to the actual when R_S is about 10^9 Ω. On the contrary, the accuracy on/off ratio measured by IDS at whole R_S range (10^2–10^{10} Ω). These results show that IDS is suitable for sensors with a wide range of resistance than TS. In addition, the on/off ratio measured by TS and IDS as functions of *f* is shown in Fig. 3f. Compared with TS, the on/off ratio in IDS is insensitive to *f*, indicating that the enhanced powering performance of TENG by IDS not influenced by frequency *f*. Also, the triboelectric layer materials, contact force of the triboelectric layer, environmental relative humidity, and the long-term operation of the TENG were investigated, as shown in Supplemental Figs. 9–11 (Supplemental Notes 9–11). The results show that the IDS has strong anti-interference capabilities, can enhance the powering performance of the TENG and achieve accurate sensing. Meanwhile, IDS is insensitive to the structure of TENGs (Supplementary Fig. 12 and Supplementary Note 12). It is worth noting that similar investigations are also carried out to evaluate the multi-mode sensing performance of a self-powered system composed of TENG and multiple sensors based on TS and IDS, and verify the validity of IDS on enhancing the powering performance of TENG for multi-mode sensing (Supplementary Fig. 13 and Supplementary Note 13).

Practical demonstration of IDS

To demonstrate IDS's availability in practical applications, the sensing performance of self-powered system composed of TENG and sensors is further investigated in Fig. 4. Here, we take commercial opto-sensors as an example. The *I-V* characteristic of the opto-sensor powered by a constant voltage source (CVS) is shown in Fig. 4a, indicating that the sensor is a kind of resistive sensor, and the resistance of the opto-sensor (R_S) is about 14.63 MΩ and 0.17 MΩ under dark and light (3.1 mW/cm^2), respectively. Following the summarized criterion ($R_{S\text{-}min} \geq 10R_F$) from Fig. 3, R_F of 10 kΩ is selected here. A dynamic light response measured by IDS, TS and CVS under eight cyclic tests switched between dark and light (1.9 mW/cm^2) are shown in Fig. 4b. An expected phenomenon was observed that I_S measured by TS hardly fluctuated, and I_S measured by IDS and CVS changed significantly. The on/off ratios of opto-sensor measured by IDS, TS and CVS are plotted in Fig. 4c. The on/off ratio measured by IDS is about 46.1, almost equal to that 49.1 by CVS, much higher than that 1.1 by TS. In addition, the sensing performance of sensor powered by IDS, TS and CVS under different light intensities is also measured in Fig. 4d. It can be found that TS performs poorly under different light intensities ranging from

https://doi.org/10.1038/s41467-025-61166-6

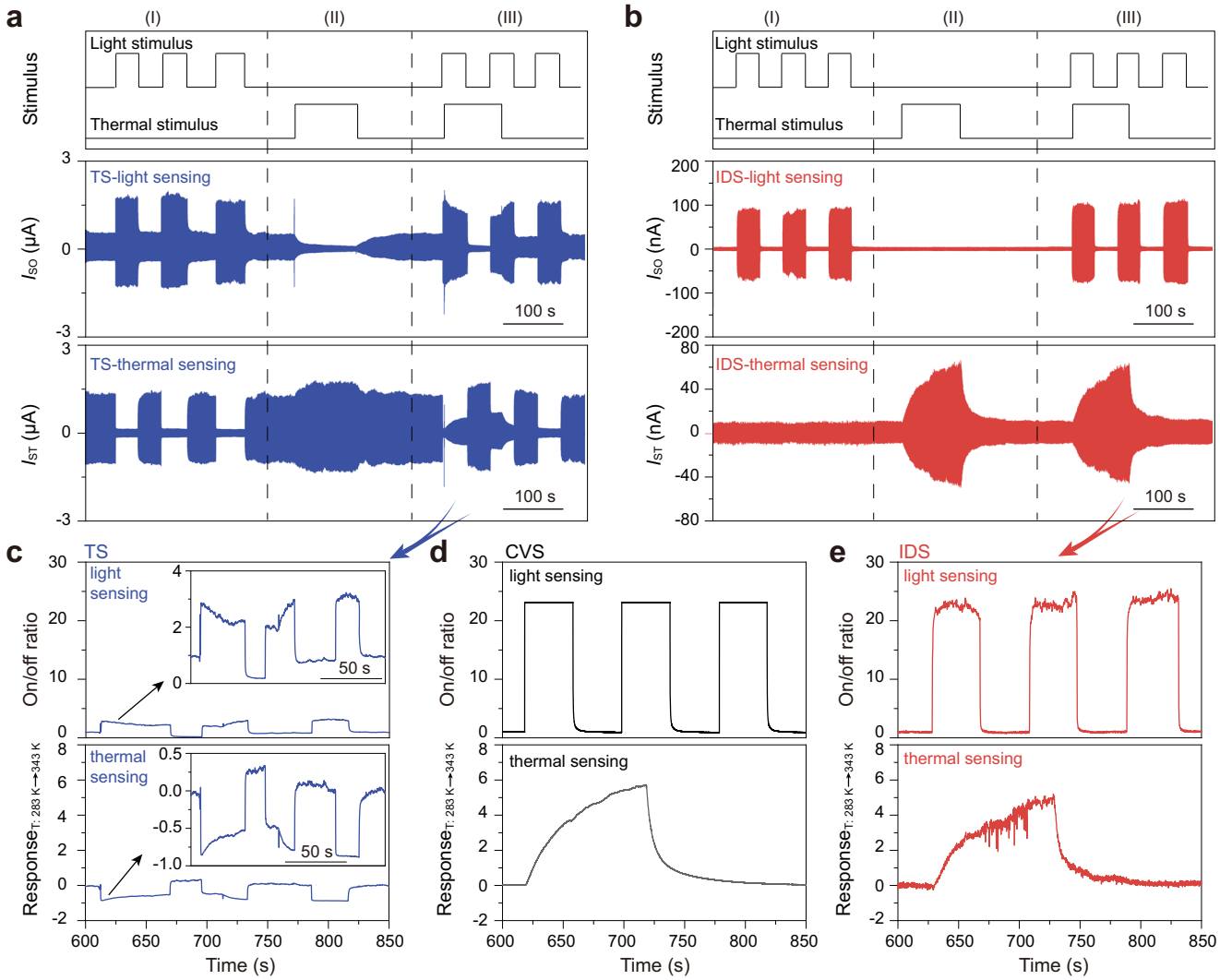

Fig. 5 | Practical demonstration of self-powered system for multi-mode sensing based on impedance decoupling strategy (IDS). a, **b** Dynamic current (I_{S1} and I_{S2}) of multi-mode sensing measured by traditional strategy (TS, **a**) and IDS (**b**). Schematic diagram of applied light and temperature stimulus in the upper part of (**a**,**b**). I_{S1} and I_{S2} fluctuation in IDS is consistent with the stimulus, while I_{S1} and I_{S2} in TS is significantly different from the stimulus. **c**–**e** Light and temperature sensing in stimuli (III) were measured by TS (**c**), constant voltage source (CVS, **d**), and IDS (**e**). Inset in c is an enlarged response curve. Light and temperature sensing measured by IDS is consistent with CVS, which indicates light and temperature sensing influence each other in TS, while in IDS they do independent.

0.2 to 3.1 mW/cm^2; while IDS performs well and can be comparable to the commercial CVS. Due to the change of mechanical energy frequency f in the environment, the powering performance of TENG in TS and IDS at different f (1 to 8 Hz) was studied. The on/off ratio measured by TS and IDS are presented in Fig. 4e. Surprisingly, as f increases, the on/off ratio measured by IDS remains stable, with a value almost equal to the intrinsic on/off ratio of the sensor. The experimental results show that IDS highly enhances the real-time powering performance of TENG, and has the ability to real-timely power the sensor with accurate sensing performance.

To further ensure the reliability of the evaluation, the on/off ratios of 20 commercial opto-sensors were measured by IDS, TS and CVS are shown in Fig. 4f. The on/off ratio of sensors powered by TENG in IDS is almost identical to that by CVS and much higher than that by TENG in TS. In addition, IDS is also applied to self-powered temperature sensing to evaluate its universal nature. Similar to light sensing, 20 commercial temperature sensors were also used for demonstration, and the sensor characteristic is shown in Supplementary Fig. 14 (Supplementary Note 14). As shown in Fig. 4g, the response (numerically equal to the on/off ratio minus 1) obtained by IDS and CVS are consistent with each other. The relative errors of temperature sensing and light sensing in IDS follow normal distributions (IDS: mean ± SD = −4.6% ± 14.1%, N = 40; TS: mean ± SD = −97.7% ± 1.2%, N = 40, SD represents standard deviation) as summarized in Fig. 4h. These evaluations regarding light sensing and temperature sensing show that IDS enables accurate sensing with overall relative error as low as −4.6%, much lower than TS (~ −97.7%). This indicates that IDS can enhance the real-time powering performance of TENG, comparable to commercial CVS. Moreover, commercial piezoresistive sensor, self-made ZnO piezoelectric strain sensor and self-made ZnO ultraviolet sensor are measured by IDS. This experiment results show that IDS can enhance the powering performance of TENG and obtain accurate sensing information, which is comparable to commercial CVS (Supplementary Figs. 15–17 and Supplementary Notes 15–17). It is worth nothing that, although IDS is only applied to five types of sensors as demonstration here, it is a universal strategy applicable to enhance real-time powering performance of TENG for other types of sensors.

Practical demonstration of self-powered system for multi-mode sensing based on IDS

As shown in Fig. 5, a self-powered system for multi-mode sensing based on IDS was further constructed for simultaneously sensing light

intensity and temperature. Dynamic current of opto-sensor (I_{SO}) and temperature sensor (I_{ST}) of multi-mode sensing measured by TS and IDS are shown in Fig. 5a, b, respectively. The programed stimuli are shown in the upper part of Fig. 5a, b, which are divided into three parts: only light without heat (I), only heat without light (II), and both heat and light (III). In TS, when the stimulus is (I), it can be clearly observed that I_{SO} increases under light stimulus, while I_{ST} decreases without thermal stimulus, which should ideally not change. Similar problems also occur in stimuli (II) and (III). The main reason for the above problems is that, taking stimulus (I) as an example, the resistance of opto-sensor (R_{SO}) decreases under light stimulation, resulting in a decrease in voltage (V_{SO}) across the opto-sensor. At the same time, the resistance of temperature sensor (R_{ST}) remains unchanged, and I_{ST} decreases with the decrease in voltage-drop across the temperature sensor (V_{ST}, $V_{SO} = V_{ST}$). In other words, the opto-sensor and temperature sensor in TS show strong crosstalk with each other, resulting in inaccurate sensing. In short, TS cannot be used for self-powered multi-mode sensing. In contrast, IDS don't show above problems. No matter it is an opto-sensor or a temperature sensor, the current changes are consistent with the applied stimulus, and two sensors work without any crosstalk. Moreover, the on/off ratio of opto-sensor and the response of temperature sensor measured by TS, CVS and IDS under stimulus (III) are summarized in Fig. 5c–e, respectively. As can be seen, the on/off ratio (response) measured by TS is smaller than IDS and CVS, and completely inconsistent with applied stimulus; as a comparison, the on/off ratio (response) measured by IDS is consistent with the applied stimulus and the on/off ratio (response) by CVS. Therefore, IDS indeed enhances the real-time powering performance of TENG, it is even also comparable to CVS for multi-mode sensing.

Discussion

In summary, a universal impedance decoupling strategy that introduces a fixed resistor to cut off the impedance coupling between TENG and sensor network is proposed and developed to enhance the real-time powering performance of TENG. Based on this strategy, self-powered systems composed of TENG and various sensor network (to monitor temperature, light, UV, force, and strain) achieves high accurate sensing performance with relative errors as low as −4.6%, and enables multi-mode sensing without any crosstalk, making TENG comparable to a commercial constant voltage source in real-time powering performance. This work provides a simple but universal strategy to enhance the powering performance of TENG for single node, multi-node or multi-mode sensing, which will greatly promote TENG toward practical applications in sensing.

Methods

Preparation of PA solution and PVDF solution

PA (Polyamide) solution and PVDF (Poly vinylidene fluoride) solution were used to respectively synthesize PA film and PVDF film, which form the triboelectric layers of TENGs[27]. PA solution consisted of 2.000 g PA and 8.000 g formic acid, which was stirred in a triangular flask for 1 h at room temperature until the solution was homogeneous. PVDF solution was prepared by dissolving 3.750 g PVDF powder in a mixed solution of 8.500 g N, N-dimethylacetamide and 12.750 g acetone, stirring at 60 °C for 30 min until homogenized.

Fabrication of TENGs

Cr/Ag electrodes (3.0 cm × 3.0 cm) were deposited on one surface of the PET (Polyethylene terephthalate) film (5.0 cm × 5.0 cm, 10 μm thick) cleaned with alcohol. Then, the PA solution and PVDF solution were spin coated (speed: 2000 r/min for PA, 5000 r/min for PVDF) on the other surface of the PET film, dry at room temperature. Finally, copper wires were connected to the Cr/Ag electrodes as output lines, and was packaged with transparent tape. The PET attached with PA film and the PET attached with PVDF film were assembled into TENGs.

Commercial sensors

Commercial temperature sensors (MF58) and opto-sensors (5549) were purchased from Yunyida Electronics Co., Ltd., Chuanju Electronics Co., Ltd., Zave Electronics Co., Ltd., respectively. The testing range of temperature sensors is from −40 to 300 °C, and its testing accuracy is 0.1 °C. The light intensity range of opto-sensors is 0 to 10 mW/cm^2, and its testing accuracy is 0.01 mW/cm^2.

Measurements of TENGs and commercial sensors

The sensing current was measured by a data acquisition card (National Instruments BNC-2120) together with a current amplifier (Stanford Research Systems Model SR570). In the measurements of commercial sensors and multi-mode sensing system, a TENG and a commercial constant voltage source (Stanford Research Systems Model DS345) were used to power commercial sensors and multi-mode sensing system, and current amplifiers were used to measure the current passing through the sensors. The commercial sensors were stimulated by heating plates, flashlights.

Data availability

All data needed to evaluate the conclusions in the paper are presented in the paper. Additional data related to this paper are available from the corresponding author upon request. Source data are provided with this paper. Source Data file has been deposited in Figshare under accession code https://doi.org/10.6084/m9.figshare.29145461[28].

References

1. Su, Q. et al. A stretchable and strain-unperturbed pressure sensor for motion-interference-free tactile monitoring on skins. *Sci. Adv.* **7**, eabi4563 (2021).
2. Zhou, Z. et al. Sign-to-speech translation using machine-learning-assisted stretchable sensor arrays. *Nat. Electron.* **3**, 571–578 (2020).
3. Hu, H. et al. A wearable cardiac ultrasound imager. *Nature* **613**, 667–675 (2023).
4. Lin, M. et al. A fully integrated wearable ultrasound system to monitor deep tissues in moving subjects. *Nat. Biotechnol.* **42**, 448–457 (2023).
5. Wang, S. et al. Skin electronics from scalable fabrication of an intrinsically stretchable transistor array. *Nature* **555**, 83–88 (2018).
6. Yang, F. et al. Wafer-scale heterostructured piezoelectric bio-organic thin films. *Science* **373**, 337–342 (2021).
7. Tang, W. et al. Microheater integrated nanotube array gas sensor for parts-per-trillion level gas detection and single sensor-based gas discrimination. *ACS Nano* **16**, 10968–10978 (2022).
8. Liu, R. Wang, Z. L., Fukuda, K. & Someya, T. Flexible self-charging power sources. *Nat. Rev. Mater.* **7**, 870–886 (2022).
9. Zou, Y. et al. A bionic stretchable nanogenerator for underwater sensing and energy harvesting. *Nat. Commun.* **10**, 2695 (2019).
10. Wen, Z., et al. Self-powered textile for wearable electronics by hybridizing fiber-shaped nanogenerators, solar cells, and supercapacitors. *Sci. Adv.* **2**, e1600097 (2016).
11. Xu, S. et al. Self-powered nanowire devices. *Nat. Nanotechnol.* **5**, 366–373 (2010).
12. Zhang, C. et al. Conjunction of triboelectric nanogenerator with induction coils as wireless power sources and self-powered wireless sensors. *Nat. Commun.* **11**, 58 (2020).
13. Liu, Y. et al. Conductive elastic sponge-based triboelectric nanogenerator (TENG) for effective random mechanical energy harvesting and ammonia sensing. *Nano Energy* **79**, 105422 (2021).
14. Han, L. et al. Self-driven photodetection based on impedance matching effect between a triboelectric nanogenerator and a MoS_2 nanosheets photodetector. *Nano Energy* **59**, 492–499 (2019).
15. Zhang, H. et al. Eco-friendly triboelectric nanogenerator for self-powering stacked In_2O_3 nanosheets/PPy nanoparticles-based NO_2 gas sensor. *Nano Energy* **128**, 109978 (2024).

16. Xia, Y. et al. Synchronous switching strategy to enhance the real-time powering and charging performance of triboelectric nanogenerator. *Adv. Mater.* **36**, e2403361 (2024).
17. Cheng, B. et al. High performance temperature difference triboelectric nanogenerator. *Nat. Commun.* **12**, 4782 (2021).
18. Niu, S. et al. Theoretical study of contact-mode triboelectric nanogenerators as an effective power source. *Energy Environ. Sci.* **6**, 3576–3583 (2013).
19. Qin, Y., Wang, X. & Wang, Z. L. Microfibre–nanowire hybrid structure for energy scavenging. *Nature* **451**, 809–813 (2008).
20. Wang, J., Li, P., Kang, X., Li, Z. & Dai, S. Soft-soft contact TENG using nonlinear coupling galloping phenomenon for harvesting wind energy. *Nano Energy* **133**, 110471 (2025).
21. Aliyana, A. K., Yang, D. & Stylios, G. K. Enhancing fabric TENG performance through optimized compression mechanics in smart IoT carpets, for energy harvesting and movement sensing. *Nano Energy* **134**, 110568 (2025).
22. Li, S. et al. Enhanced performance of TENG through graphene oxide and transition layer coupling: Achieving green energy harvesting and powering wearable devices. *Nano Energy* **133**, 110436 (2025).
23. Yao, Y. et al. Pd nanoislands-modified ZnO nanowire-network for sensitive and linear hydrogen sensing. *Nano Energy* **133**, 110512 (2025).
24. Yu, Q. et al. Highly sensitive strain sensors based on piezotronic tunneling junction. *Nat. Commun.* **13**, 778 (2022).
25. Ge, R., Yu, Q., Zhou, F., Liu, S. & Qin, Y. Dual-modal piezotronic transistor for highly sensitive vertical force sensing and lateral strain sensing. *Nat. Commun.* **14**, 6315 (2023).
26. Xu, X. et al. A real-time wearable UV-radiation monitor based on a high-performance *p*-CuZnS/*n*-TiO_2 photodetector. *Adv. Mater.* **30**, 1803165 (2018).
27. Cheng, L., Xu, Q., Zheng, Y., Jia, X. & Qin, Y. A self-improving triboelectric nanogenerator with improved charge density and increased charge accumulation speed. *Nat. Commun.* **9**, 3773 (2018).
28. Sun, H. et al. Impedance decoupling strategy to enhance the real-time powering performance of TENG for multi-mode sensing. *Figshare* https://doi.org/10.6084/m9.figshare.29145461 (2025).

Acknowledgements

This work was supported by the National Natural Science Foundation of China (Nos. 52102173 [Liu], 52472164 [Liu]), the Natural Science Foundation of Gansu Province of China (No. 23JRRA1101 [Liu]), and the National Key R & D Project from Minister of Science and Technology (2021YFA1201602 [Qin]).

Author contributions

S.H.L. and Y.Q. designed the project. H.S. performed most of the simulations and experiments. Y.X.X. contributed to simulations, and J.Y.Z. contributed to the experiments. H.S., Y.X.X., J.Y.Z., J.M., J.W.C., Z.K.C., and W.H.G. contributed to the experiment setups. H.S., S.H.L. and Y.Q. analyzed the results and prepared the manuscript. All authors have discussed the results, commented on the manuscript, and approved the final version of the manuscript.

Competing interests

The authors declare no competing interests.

Additional information

Supplementary information The online version contains supplementary material available at https://doi.org/10.1038/s41467-025-61166-6.

Correspondence and requests for materials should be addressed to Shuhai Liu or Yong Qin.

Peer review information *Nature Communications* thanks Zhen Wen and the other anonymous reviewer(s) for their contribution to the peer review of this work. A peer review file is available.